12th International Symposium on Turbulence and Shear Flow Phenomena (TSFP12)
Osaka, Japan (Online), July 19-22, 2022

THREE-DIMENSIONAL TRANSITION OF A LOW REYNOLDS NUMBER FLOW PAST A PLUNGING NACA 0012 AIRFOIL AT POST-STALL ANGLE OF ATTACK

An-Kang Gao
Department of Aeronautics
Imperial College London
London SW7 2AZ, UK
ankang.gao@imperial.ac.uk

Spencer J. Sherwin
Department of Aeronautics
Imperial College London
London SW7 2AZ, UK
s.sherwin@imperial.ac.uk

Chris D. Cantwell
Department of Aeronautics
Imperial College London
London SW7 2AZ, UK
c.cantwell@imperial.ac.uk

ABSTRACT

The two-dimensional to three-dimensional transition of a flow past a plunging NACA 0012 airfoil at a Reynolds number of $Re = 400$, based on the chord length c, and an angle of attack of 15 degrees was investigated using global linear stability analysis and spanwise-homogeneous direct numerical simulation (DNS). The peak-to-peak plunging amplitude was fixed at $A/c = 0.5$ and the Strouhal number was varied from $St_c = 0.10$ to $St_c = 1.00$. This parameter regime encompasses flow phenomena of leading-edge vortex (LEV) dominated flow ($0.10 \leq St_c \leq 0.19$), almost vanishing LEV-trailing-edge vortex (TEV) interaction ($0.22 \leq St_c < 0.5$), strong previous cycle LEV-TEV interaction ($0.49 \leq St_c \leq 0.95$) and aperiodic flow ($St_c \geq 0.99$). For the periodic baseflow, Floquet stability analysis was conducted. Below a Strouhal number of 0.5, the Floquet multiplier is smaller than the static airfoil which indicates the plunging motion stabilises the two-dimensional baseflow. For higher frequencies, a period-doubling mode appears, which has a peak Floquet multiplier around a spanwise wavelength of $2c$. This unstable mode also dominates in three-dimensional direct numerical simulations (DNS). Finally, a short-wave mode becomes unstable at $St_c = 0.95$, which generates more small-scale vorticies in the DNS result.

Introduction

For insects flying at low Reynolds numbers, the flapping wing is a common form of motion. By flapping its wings, the insect can achieve a much higher lift than the classical static wing (Ellington *et al.*, 1996) and a greater maneuverability (Alexander, 1986). This motivates the study of this mechanism and to develop smaller bio-inspired aerial vehicles.

As the simplest form of flapping, the pure plunging motion has been studied extensively. Thrust generation of a plunging airfoil at zero angle of attack (AoA) was studied by Triantafyllou *et al.* (1991); Wang (2000); Godoy-Diana *et al.* (2008) and Andersen *et al.* (2017). It was found that this gain in thrust is caused by the suction force of the leading-edge vortex (Wang, 2000) and that the critical frequency of the drag-to-thrust transition follows that of the von Kármán, to reverse von Karman, vortex street transition (Godoy-Diana *et al.*, 2008). The lift enhancement of a post-stall airfoil by the plunging motion was studied by Cleaver *et al.* (2011) both experimentally and numerically, however, the explanation of this lift enhancement through vortex dynamics has not been fully explored and so this is one of the focus of this paper.

An obvious starting point for numerical simulations is a purely two-dimensional (2-D) flow. Visbal (2009) undertook large-eddy simulations of a plunging low-aspect-ratio SD7003 airfoil at Reynolds numbers in the range 10 000 to 40 000 and showed that the three-dimensional (3-D) force is almost the same as the 2-D force at a reduced frequency of $St_c = 1.25$ and a normalised amplitude of $A/c = 0.1$, where c is the chord length. Zurman-Nasution *et al.* (2020) conducted direct numerical simulations of a flapping NACA 0016 airfoil at a Reynolds number of 5300 and found the 2-D force only to be valid for a range of Strouhal numbers around $St_c = 0.3$ for pure plunging motions.

The transition boundary and mechanism of 2-D to 3-D flow are clearly crucial for assessing the validity of 2-D simulations. Moriche *et al.* (2016) studied the global instability of a combined plunging and pitching NACA 0012 airfoil at a Reynolds number of 1000 and an amplitude of $2c$. They found a long-wave subharmonic unstable mode, which has a peak Floquet multiplier at a wavelength of $4.078c$ and resembles mode A of the cylinder flow. Sun *et al.* (2018) studied the instability of a plunging NACA 0015 airfoil at zero angle of attack, a Reynolds number of 1700, amplitudes from 0 to $0.3c$ and reduced frequencies from 4 to 8.4. They found three unstable modes: mode A, a quasi-periodic mode, and mode B, but the quasi-periodic mode is not dominant in the transition region.

This study aims to explore the 2-D to 3-D transition mechanism of a very low Reynolds number ($Re = 400$) flow past a post-stall NACA 0012 airfoil. The plunging amplitude is fixed at $0.5c$ which is between the amplitude used by Moriche *et al.*

(2016) and Sun *et al.* (2018). The plunging frequency is increased gradually from below the natural shedding frequency to chaotic flow, to cover the complete range of flow regimes. Direct numerical simulations are also conducted. The link between linear stability analysis and direct numerical simulations is further discussed.

Numerical methods

The airfoil is treated as a rigid body with a fixed angle of attack (AoA) of 15 degrees. To avoid the need for a moving grid, the absolute velocity $\boldsymbol{u}$ is solved in the body frame of reference. The governing equations in dimensionless form are

$$\nabla \cdot \boldsymbol{u} = 0, \tag{1}$$

$$\partial_t \boldsymbol{u} + (\boldsymbol{u} - \boldsymbol{U}_B) \cdot \nabla \boldsymbol{u} = -\nabla p + Re^{-1} \nabla^2 \boldsymbol{u}. \tag{2}$$

In this study, $Re = 400$ is based on the uniform incoming flow $U_\infty = 1$ and the chord length $c = 1$. The airfoil moves transversely under the motion

$$\boldsymbol{U}_B = -\pi A f \sin(2\pi f t) \boldsymbol{e}_y, \tag{3}$$

where f is the plunging frequency and $A = 0.5c$ is the peak-to-peak amplitude.

Two dimensionless frequencies can be defined. These are the reduced frequency, which is usually used to measure the flow unsteadiness, given by

$$k = \pi f c / U_\infty, \tag{4}$$

and the Strouhal number,

$$St_c = k/\pi = f c / U_\infty. \tag{5}$$

A second-order velocity correction scheme (Karniadakis *et al.*, 1991) is used to transform equations (1) and (2) into a set of Helmholtz equations (one for each space dimension) and one pressure Poisson equation. The spectral/*hp* element method, which is implemented in the open-source code, Nektar++ (Cantwell *et al.*, 2015), is used to solve equations (1) and (2).

The computational domain spans $-40 \leq x \leq 60$, $-40 \leq y \leq 40$ and contains 9985 quadrilateral and 64 triangular elements, with 5 polynomial modes in each dimension. The height of the first layer elements on the body surface is enforced to be $0.005c$. For the spanwise-homogeneous 3-D simulation, a Fourier expansion with de-aliasing is applied. The spanwise length is $10c$ and 64 Fourier planes are used (32 complex modes). A spectral vanishing viscosity (SVV) with a DG-mimic kernel (Moura *et al.*, 2020) is also applied in the polynomial expansion to improve numerical stability. Based on the parameters in Son *et al.* (2022), the above resolution is sufficient.

The linearised equation (2) with infinitesimal 3-D disturbance is also solved in order to explore the linear stability of the periodic baseflow. According to Floquet theory, an eigenmode can be assumed to have the following form

$$u(x,y,z,t_0+nT) = \mu^n \hat{u}(x,y,t_0)\cos(\beta z), \tag{6}$$

$$v(x,y,z,t_0+nT) = \mu^n \hat{v}(x,y,t_0)\cos(\beta z), \tag{7}$$

$$w(x,y,z,t_0+nT) = \mu^n \hat{w}(x,y,t_0)\sin(\beta z). \tag{8}$$

Here, μ is the Floquet multiplier and $|\mu| > 1$ indicates an unstable mode. $\beta = 2\pi/\lambda$ is the wavenumber and λ is the wavelength. A modified Arnoldi algorithm with an iteration tolerance of 10^{-5} is used to find the most unstable eigenvalue and eigenmode (Barkley *et al.*, 2008). The periodic baseflow is captured by 128 snapshots over one time period and interpolated using 4th-order Lagrange interpolation.

Results

The time-averaged lift and drag coefficients at $Re = 400$, $A/c = 0.5$, are shown in Figure 1. For comparison, experimental force coefficients of Cleaver *et al.* (2011) at $Re = 10000$, $A/c = 0.4$, and implicit large-eddy simulation results of Son *et al.* (2022) at $Re = 10000$, $A/c = 0.5$, are also presented.

For $St_c < 0.5$, both the lift and the drag forces increase with plunging frequency. Around $St_c = 0.32$ ($k = 1$), the low-Reynolds number lift agrees with high-Reynolds number results and the lift is insensitive to the plunging amplitude. The low-Reynolds number drag is larger than the high-Reynolds number results due to stronger friction.

A jump in the forces exists around $St_c = 0.5$ with a hysteresis from $St_c = 0.49$ to 0.5. The lift on the left side is 1.2 times higher than the lift on the right side of the jump. On the left branch, the 3-D flow is the same as the 2-D flow and therefore no 3-D data is given there. On the right branch, the 3-D flow deviates from the 2-D flow. This indicates the 2-D flow becomes unstable in the low-lift right hand branch.

For $St_c > 0.5$, the lift from the numerical simulations is smaller than the experimental result of Cleaver *et al.* (2011). However, the 3-D lift is higher than the 2-D lift. The drag decreases with plunging frequency and transitions to thrust around $St_c = 0.76$ ($k = 2.4$). The 3-D low-Reynolds number drag agrees with the high-Reynolds number result.

2-D baseflow

The wake pattern of the 2-D baseflow is shown in Figure 2. Based on the streamwise advection length of the LEV and the vortex interactions, the Strouhal number range can be classified into four regions.

Region 1 corresponds to $0.10 \leq St_c \leq 0.19$ ($0.3 \leq k \leq 0.6$). In this St_c range, the streamwise advection length of the LEV during a half period is longer than the chord length c. One strong trailing-edge vortex (TEV) sheds when the LEV passes the trailing edge and several small TEVs also shed between two successive LEVs.

Region 2 corresponds to $0.22 \leq St_c < 0.5$ ($0.7 \leq k < 1.57$). In this range, the streamwise advection length of the LEV during a half period is shorter than c but the advection length during one period is longer than c. The interaction between the LEV and the TEV is very weak. For $0.22 \leq St_c \leq 0.38$ ($0.7 \leq k \leq 1.2$), the TEV is positioned nearly equidistant between the current LEV and the previous LEV (pLEV). Interaction between the LEV and the pLEV is also weak. Two single vortices are shed in each period and no vortex pair is formed. Vortices in the wake align along a straight line. In this St_c range, the flow is insensitive to the Reynolds number and the plunging amplitude, and the 2-D flow is stable, as can be seen by a comparison between the present vorticity fields at $Re = 400$ and the PIV results of Son *et al.* (2022) at $Re = 10000$ in Figure 3. The stable 2-D flow around $k = 1$ is also confirmed by Zurman-Nasution *et al.* (2020). For $0.41 \leq St_c < 0.5$ ($1.3 \leq k < 1.57$), the pLEV interacts with the TEV and forms a vortex pair in the wake. In this vortex pair,

St_c	k	λ/c	μ
0.50	1.57	2 ± 0.06	-1.0569
0.64	2.00	2 ± 0.07	-1.6519
0.80	2.50	1.8 ± 0.3	-1.7205
0.95	3.00	1.8 ± 0.3	-2.0912

Table 1. The most unstable wavelength and the corresponding Floquet multiplier at $Re = 400, A/c = 0.5$.

the pLEV is stronger than the TEV. Therefore, their induced motion leads to this vortex pair moving upwards.

Region 3 corresponds to $0.49 \leq St_c \leq 0.95$ ($1.53 \leq k \leq 3.00$). In this range, the 2-D flow is still periodic but the advection length of the LEV during one period is shorter than the chord length c. The TEV has enough time to grow as the pLEV starts interacting with it. Therefore, the TEV is stronger in the vortex pair, forming a downward motion pLEV-TEV vortex pair in the wake. The induced velocity of this vortex pair also reduces the strength of the current LEV. As a result, the lift, which is correlated with the LEV, is also reduced.

Region 4 corresponds to $St_c \geq 0.99$ ($k \geq 3.1$). In this range, the 2-D baseflow becomes aperiodic.

Linear stability result

The linear stability results are shown in Figure 4. To test the convergence of the numerical result, a refined mesh with 7 polynomial modes and a baseflow with 256 snapshots are also used and are shown as red circles. The relative difference is within 1%.

For $St_c < 0.5$ ($k < 1.57$), no absolute unstable mode is observed. For $St_c \geq 0.49$ ($k \geq 1.53$), a periodic-doubling mode (μ is a negative real number) first becomes unstable. The most unstable wavelength and the corresponding Floquet multiplier are shown in table 1. For all four frequencies explored, the most amplified mode has a wavelength of about twice the chord length. At $St_c = 0.5$ ($k = 1.57$) and 0.64 ($k = 2$), this long-wave mode has a narrow bandwidth. At $St_c = 0.80$ ($k = 2.5$), two short-wave stable modes with wavelength of about $0.7c$ and $0.3c$ appear. At $St_c = 0.95$ ($k = 3$), modes in a wide wavelength range $\lambda \geq 0.25c$ are unstable.

3-D result

Since the characteristic wavelength of the most amplified mode is around $2c$, the spanwise length of the 3-D simulation is set as $10c$, which is 5 times the wavelength. The flow is first simulated for 20 time periods using 32 planes in the spanwise direction. Then 64 planes are used to continue the simulation for another 20 time periods.

Evolution of the spanwise vorticity at $St_c = 0.64 (k = 2)$, $Re = 400$, $A/c = 0.5$, is shown in Figure 5. Both the 2-D flow and the spanwise-averaged flow are shown. At $t/T = 0.75$ when the LEV has just formed, the LEV is very strong and there is no significant displacement along the vortex column. At $t/T = 1$, the LEV in the 2-D flow has an almost circular shape, but the LEV in the 3-D flow are stretched in a 45-degree direction. The 3-D effect makes the spanwise averaged LEV appear to diffuse faster (through 3D deformations) and reduces the adverse effect of the pLEV on the lift. Therefore the 3-D lift is higher than the 2-D lift.

A spanwise probe line was placed at $x = 0.16, y = 0.16$ as shown by the white dot in figure 5. The period-doubling phenomenon is clearly shown by the time evolution of the spanwise velocity w on this probe line in Figure 6. The alternative change of the sign of w along the spanwise direction indicates the bending wave on the LEV. At $St_c = 0.64$ ($k = 2$) and $St_c = 0.80$ ($k = 2$), the flow evolution pattern is regular and periodic. At $St_c = 0.95$ ($k = 3$), the long-wave period-doubling pattern is still the most significant spanwise pattern but there are also many aperiodic small scales.

To measure the energy distribution along the spanwise wavenumber, the time-averaged power spectral density of w on the probe line is shown in Figure 7. At $St_c = 0.64$ ($k = 2$) and $St_c = 0.80$ ($k = 2$), the spanwise disturbance mainly distributed on the most energetic wavelength $\lambda = 2c$ ($\beta = \pi$) and its higher harmonics. This wavelength $2c$ agrees with the linear stability result. At $St_c = 0.95$ ($k = 3$), the most energetic wavelength is $\lambda = 1.7c$ but the power spectral density shows a continuous distribution across all wavenumbers. This is in agreement with linear stability results that the mode is unstable for a wide range of wavelengths at $St_c = 0.95$ ($k = 3$).

Conclusions

The two-dimensional (2-D) to three-dimensional (3-D) transition of a plunging airfoil at a post-stall angle of attack of 15 degrees, a Reynolds number of 400 and a plunging amplitude of $0.5c$ was explored using linear stability analysis and spanwise-homogeneous direct numerical simulations.

For $St_c < 0.5$, the lift grows with plunging frequency and the 2-D flow is stable. The lift drops to less than half of the highest value at around $St_c = 0.5$, with a hysteresis from $St_c = 0.49$ to $St_c = 0.5$. For $St \geq 0.49$, the 2-D flow is unstable. A period-doubling mode with a wavelength of approximately twice the chord length first becomes unstable. This mode is also the dominating spanwise flow structure in the fully developed 3-D flows.

Acknowledgements

The authors acknowledge the Engineering and Physical Sciences Research Council (EPSRC) Grant No. EP/S029389/1 and UK Turbulence Consortium EP/R029326/1. This work used the ARCHER2 UK National Supercomputing Service (https://www.archer2.ac.uk). The authors would also like to acknowledge HPC support from Imperial College Research Computing Service (DOI: 10.14469/hpc/2232).

REFERENCES

Alexander, D. E. 1986 Wind tunnel studies of turns by flying dragonflies. *Journal of Experimental Biology* **59** (3), 81.

Andersen, A, Bohr, Tomas, Schnipper, Teis & Walther, Jens Honore 2017 Wake structure and thrust generation of a flapping foil in two-dimensional flow. *Journal of fluid mechanics* **812**.

Barkley, D., Blackburn, H. M. & Sherwin, S. J. 2008 Direct optimal growth analysis for timesteppers. *International Journal for Numerical Methods in Fluids* **57** (9), 1435–1458.

Cantwell, Chris D, Moxey, David, Comerford, Andrew, Bolis, Alessandro, Rocco, Gabriele, Mengaldo, Gianmarco, De Grazia, Daniele, Yakovlev, Sergey, Lombard, J-E, Ekelschot, Dirk *et al.* 2015 Nektar++: An open-source

spectral/hp element framework. *Computer physics communications* **192**, 205–219.

Cleaver, D. J., Wang, Z., Gursul, I. & Visbal, M. R. 2011 Lift enhancement by means of small-amplitude airfoil oscillations at low reynolds numbers. *AIAA Journal* **49** (9), 2018–2033.

Ellington, Charles P, Van Den Berg, Coen, Willmott, Alexander P & Thomas, Adrian LR 1996 Leading-edge vortices in insect flight. *Nature* **384** (6610), 626–630.

Godoy-Diana, Ramiro, Aider, Jean-Luc & Wesfreid, José Eduardo 2008 Transitions in the wake of a flapping foil. *Physical Review E* **77** (1), 016308.

Karniadakis, George Em, Israeli, Moshe & Orszag, Steven A 1991 High-order splitting methods for the incompressible navier-stokes equations. *Journal of computational physics* **97** (2), 414–443.

Moriche, M, Flores, O & García-Villalba, M 2016 Three-dimensional instabilities in the wake of a flapping wing at low reynolds number. *International Journal of Heat and Fluid Flow* **62**, 44–55.

Moura, Rodrigo C, Aman, Mansoor, Peiró, Joaquim & Sherwin, Spencer J 2020 Spatial eigenanalysis of spectral/hp continuous galerkin schemes and their stabilisation via dg-mimicking spectral vanishing viscosity for high reynolds number flows. *Journal of Computational Physics* **406**, 109112.

Son, Onur, Gao, A-K, Gursul, Ismet, Cantwell, Chris D, Wang, Zhijin & Sherwin, Spencer J 2022 Leading-edge vortex dynamics on plunging airfoils and wings. *Journal of Fluid Mechanics* **940**.

Sun, Liping, Deng, Jian & Shao, Xueming 2018 Three-dimensional instabilities for the flow around a heaving foil. *Physical Review E* **97** (1), 013110.

Triantafyllou, M. S., Triantafyllou, G. S. & Gopalkrishnan, R. 1991 Wake mechanics for thrust generation in oscillating foils. *Physics of Fluids A: Fluid Dynamics* **3** (12), 2835–2837.

Visbal, Miguel R 2009 High-fidelity simulation of transitional flows past a plunging airfoil. *AIAA journal* **47** (11), 2685–2697.

Wang, Z. J. 2000 Vortex shedding and frequency selection in flapping flight. *Journal of Fluid Mechanics* **410** (410), 323–341.

Zurman-Nasution, AN, Ganapathisubramani, Bharathram & Weymouth, GD 2020 Influence of three-dimensionality on propulsive flapping. *Journal of Fluid Mechanics* **886**.

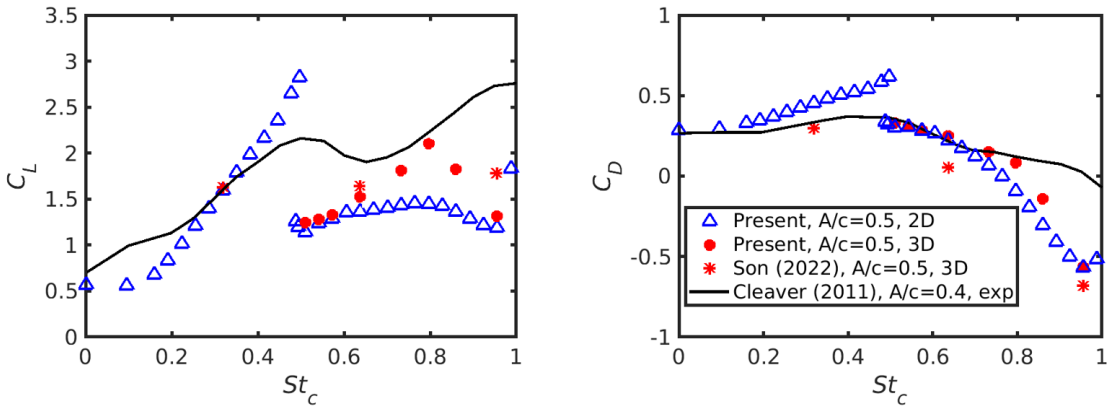

Figure 1. Time-averaged lift and drag coefficient scaled by $0.5\rho U_\infty^2 c$ of the plunging airfoil. In present simulations, $Re = 400$. In Son *et al.* (2022); Cleaver *et al.* (2011), $Re = 10000$.

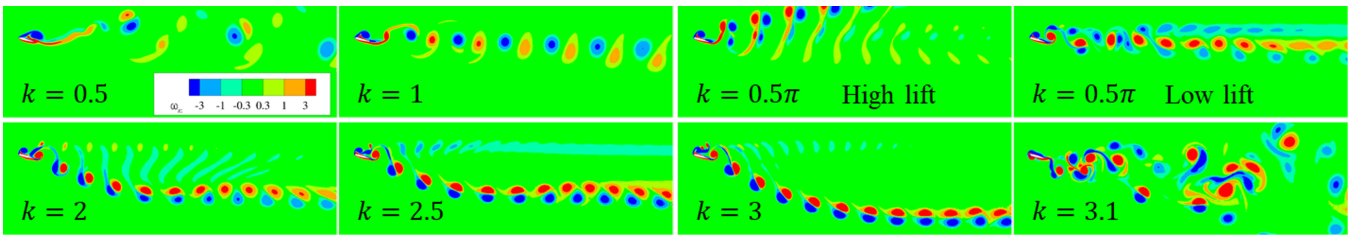

Figure 2. Wake patterns of the 2-D plunging airfoil at $Re = 400$, $t/T = 0.5$.

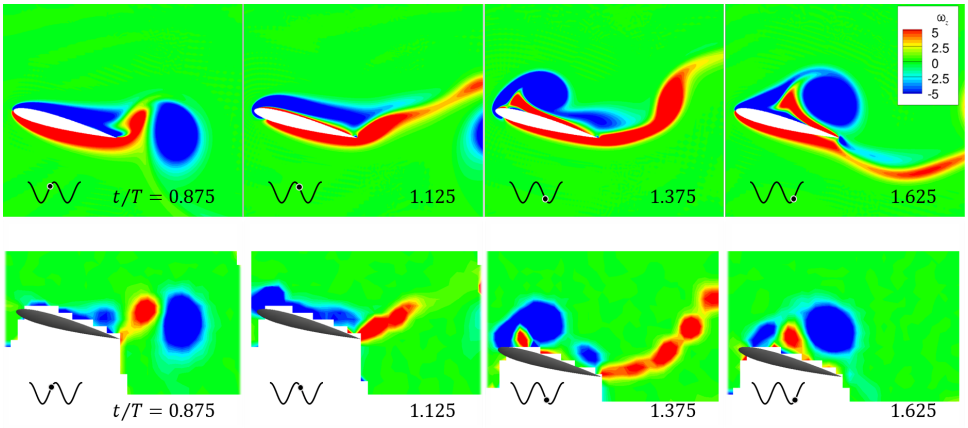

Figure 3. Upper panels: instantaneous vorticity field of the 2-D plunging airfoil at $k = 1$, $Re = 400$. Lower panels: phase-averaged vorticity field of the plunging airfoil at $k = 1$, $Re = 10000$ from Son *et al.* (2022)

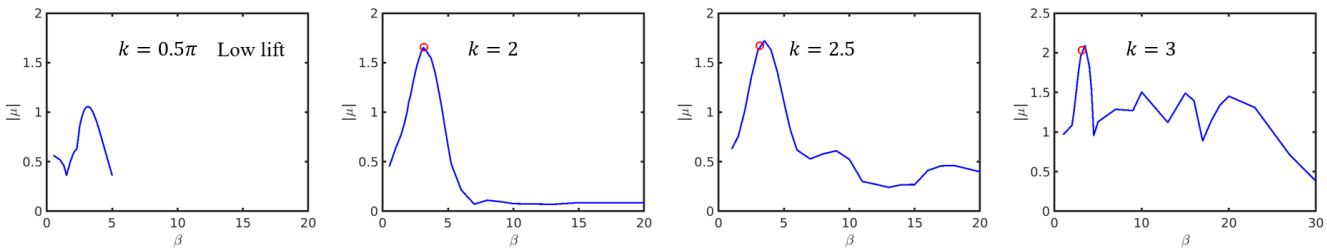

Figure 4. Floquet multiplier of the 2-D plunging airfoil at $Re = 400$. Red circles are the refined results to show numerical convergence.

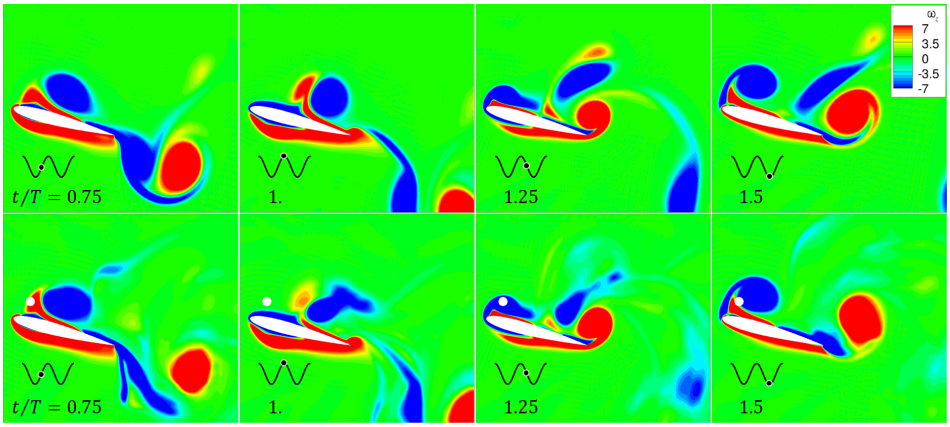

Figure 5. Upper panels: instantaneous vorticity fields of the 2-D plunging airfoil at $k = 2$, $Re = 400$. Lower panels: spanwise-averaged vorticity field of the 3-D plunging airfoil at $k = 2$, $Re = 400$.

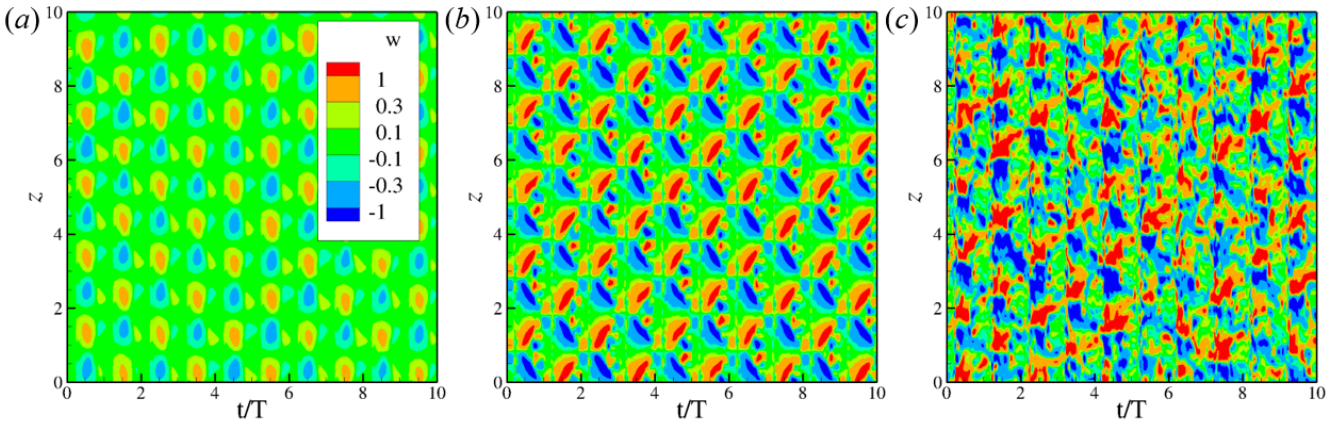

Figure 6. Evolution of the spanwise velocity on the probe line ($x = 0.16$, $y = 0.16$) for (a) $k = 2$, (b) $k = 2.5$, (c) $k = 3$.

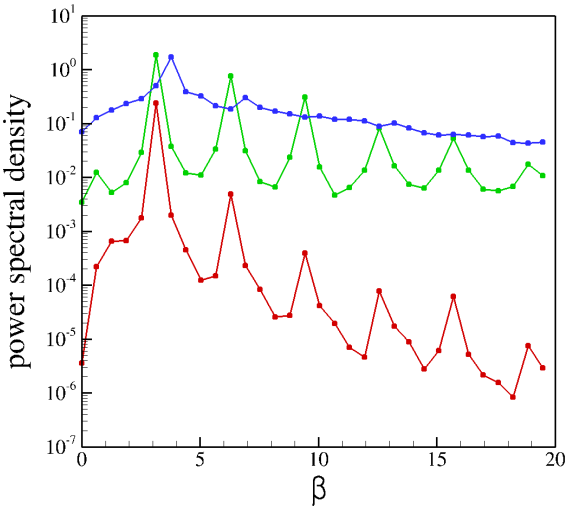

Figure 7. Power spectrum of the spanwise velocity on the probe line ($x = 0.16$, $y = 0.16$). From low to high, $k = 2$, $k = 2.5$ and $k = 3$.